Brain Pathology ISSN 1015-6305

RESEARCH ARTICLE

Stress-Induced Upregulation of SLC19A3 is Impaired in Biotin-Thiamine-Responsive Basal Ganglia Disease

Anne Schänzer[1]*; Barbara Döring[2]*; Michelle Ondrouschek[3]*; Sarah Goos[1]; Boyan K. Garvalov[1]; Joachim Geyer[2]; Till Acker[1]; Bernd Neubauer[3]; Andreas Hahn[3]

[1] Institute of Neuropathology, Justus-Liebig-University, Giessen, Germany.
[2] Institute of Pharmacology and Toxicology, Biomedical Research Center Seltersberg, Justus-Liebig-University, Giessen, Germany.
[3] Department of Child Neurology, Justus-Liebig-University, Giessen, Germany.

Keywords
Basal ganglia disease, BTBGD, Leigh's syndrome, SLC19A3, thiamine, thiamine transporter 2, Wernicke-like encephalopathy.

Corresponding author:
Andreas Hahn, MD, Department of Child Neurology, Feulgenstr. 10–12, 35392 Giessen, Germany (E-mail: *andreas.hahn@paediat.med.uni-giessen.de*)

Received 25 October 2013
Accepted 18 December 2013
Published Online Article Accepted 23 December 2013

* These authors contributed equally to the manuscript.

doi:10.1111/bpa.12117

Abstract

Biotin-thiamine-responsive basal ganglia disease (BTBGD) is a potentially treatable disorder caused by mutations in the *SLC19A3* gene, encoding the human thiamine transporter 2. Manifestation of BTBGD as acute encephalopathy triggered by a febrile infection has been frequently reported, but the underlying mechanisms are not clear. We investigated a family with two brothers being compound heterozygous for the *SLC19A3* mutations p.W94R and p.Q393*fs. Post-mortem analysis of the brain of one brother showed a mixture of acute, subacute and chronic changes with cystic and necrotic lesions and hemorrhage in the putamen, and hemorrhagic lesions in the caudate nucleus and cortical layers. *SLC19A3* expression was substantially reduced in the cortex, basal ganglia and cerebellum compared with an age-matched control. Importantly, exposure of fibroblasts to stress factors such as acidosis or hypoxia markedly upregulated *SLC19A3* in control cells, but failed to elevate *SLC19A3* expression in the patient's fibroblasts. These results demonstrate ubiquitously reduced thiamine transporter function in the cerebral gray matter, and neuropathological alterations similar to Wernicke's disease in BTBGD. They also suggest that episodes of encephalopathy are caused by a substantially reduced capacity of mutant neuronal cells to increase *SLC19A3* expression, necessary to adapt to stress conditions.

INTRODUCTION

Biotin-thiamine-responsive basal ganglia disease (BTBGD) is characterized by acute/subacute episodes of confusion, dystonia, epileptic seizures, external ophthalmoplegia, dysphagia and other neurological symptoms, which may eventually progress to coma and death if left untreated (14, 21). These symptoms are associated with distinct basal ganglia abnormalities in magnetic resonance imaging (MRI) (14, 21). Manifestation of neurological symptoms may be preceded by a febrile illness or occur during a catabolic state (2, 14, 21). Administration of high doses of biotin, thiamine or both may reverse or substantially ameliorate neurological dysfunction, albeit response to treatment has been inconsistent (2, 11, 14, 21, 22). BTBGD is caused by recessively inherited mutations in the *SLC19A3* gene encoding the human thiamine transporter 2 (THTR2), which shares 70% homology with the human thiamine transporter 1 (THTR1) encoded by *SLC19A2* (23).

In addition to BTBGD, *SLC19A3* mutations have also been reported in a newborn presenting with acute encephalopathy and lactic acidosis (16), in infants affected by Leigh's syndrome (6, 9), in four related subjects manifesting with atypical infantile spasms (22), and in two brothers with Wernicke's-like encephalopathy (11). Post-mortem studies have been performed in two infants with Leigh's syndrome and revealed multiple infarct-like lesions and a loss of neurons in the basal ganglia, and the cerebral and cerebellar cortex (9).

Functional effects on cellular thiamine uptake have been characterized for some *SLC19A3* mutations (6, 11, 19, 22). However, it is not clear by which mechanism *SLC19A3* dysfunction leads to brain lesions and neurological symptoms, and how extrinsic factors (e.g. fever, infection) may trigger episodes of encephalopathy. Here, we aimed at elucidating pathophysiological mechanisms underlying this condition. We performed mutational analyses of *SLC19A3* in two brothers affected by BTBGD, determined thiamine uptake via THTR2 in HEK293 cells, investigated histological alterations in post-mortem cerebral tissue, and examined expression of *SLC19A3* in different brain regions. Finally, *SLC19A3* expression was studied in wild type (wt) and mutant (mt) fibroblasts under hypoxic and acidic conditions. Collectively, our data indicate that BTBGD is caused by a failure of stress-induced increase in *SLC19A3* expression.

MATERIAL AND METHODS

Patients

Two brothers with the clinical presentation of an encephalopathy with main involvement of the basal ganglia were identified.

Mutation analyses were performed from the brothers and the parents. Post-mortem analyses, including *SLC19A3* expression in different regions of the brain, were done in one brother and were compared with an age-matched control brain. Cultured fibroblasts from the patient with BTBGD were analyzed for thiamine uptake and expression for *SLC19A3* under stress-induced conditions. Written informed consent was obtained from all subjects or their legal guardians according to the study protocols approved by the institutional review boards of the University Giessen, Germany.

Mutational analysis

The *SLC19A3* gene was amplified by Qiagen Multiplex polymerase chain reaction (PCR) Kit and by Expand Long Range PCR Kit (Roche, Mannheim, Germany) on a Biometra T3 thermocycler. Sequencing reactions were performed using ABI PRISM BigDye Terminator v3.1 Cycle Sequencing Kit (Applied Biosystems, Weiterstadt, Germany). Capillary electrophoresis was conducted on an ABI PRISM 3100 Genetic Analyzer (Applied Biosystems). Quantitative real-time PCR was performed by the TaqMan Copy Number Assay method (Applied Biosystems). To determine the relative copy number of a genomic sequence of interest, TaqMan Copy Number Assays were run together with a TaqMan Copy Number Reference Assay in a duplex real-time PCR on every single *SLC19A3* exon. RNA was isolated from wt and patient fibroblasts using RNeasy Plus Mini Kit (Qiagen, Hilden, Germany) and reverse-transcribed with SuperScript II Reverse Transcriptase (Invitrogen, Karlsruhe, Germany) and oligo dT primers (Invitrogen). Synthesized cDNA was amplified by PCR using Fast Start High Fidelity Polymerase (Roche) for sequencing and cloning into pcDNA5/FRT/V5-His-TOPO vector (Invitrogen).

Neuropathological examination

The brain of patient 2 was fixed in 4% paraformaldehyde and cut in coronal sections. Tissue samples were processed using standard protocols. Five-micrometer-thin paraffin sections were stained with hematoxylin and eosin (H&E) and prussian blue (iron). Immunohistochemistry was performed with a Bench Mark XT automatic staining platform (Ventana, Heidelberg, Germany) using the following antibodies: anti-NeuN (MAB377, Chemicon, Limburg, Germany), anti-glial fibrillary acidic protein (GFAP) (Z0334, DAKO, Hamburg, Germany), anti-CD31 (M0823, DAKO), anti-CD68 (M0876, DAKO), anti-CD45 (M0701, DAKO), anti-CD3 (RM9107, Medac, Gräfelfing, Germany), anti-CD8 (M7103, DAKO) and anti-CD20 (M0755, DAKO). For electron microscopy, the tissue samples were fixed in 3.9% glutaraldehyde, processed with a Leica EM TP tissue processor and contrasted with a Leica EM AC20 instrument (ultrastain kit, Wetzlar, Germany). From plastic-embedded tissue, 1–2 μm thin sections were stained with methylene blue (MB). Ultrathin sections were analyzed with an electron microscope (Zeiss EM 109, Fürth, Germany). Some tissues of different brain regions and liver were snap-frozen in liquid nitrogen.

Thiamine transport measurement

GripTite 293 MSR and MDCK cells (Invitrogen) were seeded in 24-well plates and transiently transfected with the untagged and V5-His tagged *SLC19A3* constructs as well as an empty vector (control) at a confluence of 80% using Lipofectamine 2000 transfection reagent (Invitrogen). After 24 h, medium was changed and protein expression was enhanced by incubation with medium containing 2 mM sodium butyrate for further 24 h. Prior to transport assays, the transfection efficiency was controlled by immunofluorescence analysis and showed similar rates for the *SCL19A3* wild type, p.W94R and p.Q393*fs constructs. In addition, no cytotoxic effects could be observed during the cultivation of transiently transfected cells over a period of 48 h. Transport measurements were performed as described before (7). Thiamine uptake was measured at concentrations of 0 μM, 10 μM, 20 μM, 30 μM, 40 μM, 50 μM, 60 μM and 70 μM in the medium.

Localization of mutant protein in MSR and MDCK cells

Immunofluorescence studies were performed on transiently transfected GripTite 293 MSR and MDCK cells grown on glass coverslips in 24-well plates as reported previously (7). In short, cells were washed in PBS, fixed in 2% paraformaldehyde (Roth, Karlsruhe, Germany) and permeabilized with 0.2% TritonX-100 (Sigma, Deisenhofen, Germany). After blocking in 1% bovine serum albumin and 4% goat serum (PAA, Cölbe, Germany) (blocking solution), cells were incubated for 1 h at room temperature with the mouse anti-V5 antibody (Invitrogen) diluted 1:5000 in blocking solution. Washed cells were incubated for 1 h at room temperature with the goat anti-mouse IgG AlexaFluor488 antibody (Invitrogen) 1:800 in blocking solution. Staining of cell nuclei was conducted with DAPI (Roche) diluted 1:5000 in methanol (Roth) for 5 minutes. Coverslips with the methanol washed and air-dried cells were mounted on slides with Prolong Gold antifade reagent (Invitrogen). Fluorescence imaging was performed using Leica DM5500B microscope with motorized Z-focus and LAS AF 6000 software with 3D deconvolution tool.

Determination of protein and mRNA expression in the brain

Unfixed brain tissue samples from different regions were analyzed from patient 2 and an age-matched control. The tissue was lysed in 10 mM Tris HCl pH 7.5, 2% SDS, 2 mM EGTA, 20 mM NaF and homogenized using an ultrasound sonifier (Sonopuls Bandelin, Berlin, Germany) and a mechanical homogenizer (T10 Ultra-Turrax, IKA, Staufen, Germany). Protein concentration was determined using the DC protein assay (Bio-Rad, Munich, Germany). Equal amounts of total protein were loaded on an SDS-PAGE gel, transferred to a Hybond ECL nitrocellulose membrane (GE Healthcare, Munich, Germany) and analyzed using the following primary antibodies: anti-SLC19A3 rabbit polyclonal antibody (NBP1–69703, Novus Biologicals, Littleton, CO, US), anti-NeuN mouse monoclonal antibody (clone A60, Millipore, Darmstadt, Germany, MAB377), anti-GFAP rabbit polyclonal antibody (Z0334, DAKO), anti-HIF-1α rabbit polyclonal antibody (10006421, Cayman Chemical, Hamburg, Germany), anti-β-actin mouse monoclonal antibody (A5316, Sigma, Frankfurt, Germany) and anti-α-tubulin mouse monoclonal antibody (DLN09992, Dianova, Hamburg, Germany). The polyclonal SLC19A3 antibody used was raised against a peptide of the SLC19A3 protein derived

from a region with low homology to SLC19A2, thus making a cross-reaction with SLC19A2 is unlikely.

To determine SLC19A3 expression by quantitative real-time PCR, RNA from patient tissues was isolated with the RotiQuick-Kit (Roth) and reverse transcribed using RevertAid H Minus M-MuLV Reverse Transcriptase (Thermo Fisher Scientific, Dreieich, Germany). cDNA was amplified using the ABsolute QPCR SYBR Green Mix or the ABsolute QPCR Mix (ABgene, Hamburg, Germany) and a StepOnePlus real-time PCR system (Applied Biosystems). The primers used for SLC19A3 quantification were as previously described (17). The difference in the threshold number of cycles between the gene of interest and hypoxanthine phosphoribosyltransferase 1 (HPRT) was then normalized relative to the standard chosen for each experiment and converted into *x*-fold difference.

Stress induction in fibroblasts

Patient and control fibroblasts were cultured in AmnioMax C-100 Medium (Invitrogen) with AmnioMax C-100 Supplement (Invitrogen). Cells were incubated in a humidified incubator at 37°C with 5% CO_2 and 21% O_2. For hypoxic treatments, the cells were incubated in a humidified hypoxic chamber (Coy Laboratory Products, Munich, Germany) at 37°C, 5% CO_2 and 1% O_2 (12). To analyze the impact of different pH, the cells were incubated in CO_2-independent medium (Gibco, Darmstadt, Germany) at physiological pH (pH 7.4, adjusted by addition of NaOH). For incubation at acidic pH, the cells were first grown at pH 7.4 for 96 h, followed by 24 h in medium with pH 6.7 (adjusted by addition of HCl). To assess the effect of biotin, cells were incubated for 24 h in AmnioMax C-100 Medium (Invitrogen) containing biotin at concentrations of 0.01 μM–10 μM.

RESULTS

Clinical presentation and MRI findings

The family is of German ancestry. The mother gave birth to three sons from three different fathers, of whom two were brothers. Patient 1 presented at age 3½ years with somnolence and generalized dystonia following a febrile upper respiratory tract infection. Symptoms progressed to coma, and hypoventilation necessitated artificial ventilation. Initial brain MRI displayed bilateral cystic swelling and increased signal intensities on T2-weighted images of the putamen and caudate nuclei (Figure 1). An acute necrotizing encephalopathy or a metabolic disorder was suspected, but extensive infectiological and neurometabolic examinations including lumbar puncture, determination of organic acids in urine, amino acids in plasma, acylcarnitine profile, lactate, pyruvate, thiamine, and biotin levels, and respiratory chain complex activities in muscle gave normal results. Signal hyperintensities partially resolved during the next weeks, but progressive cortical lesions appeared. This was accompanied by prolonged multifocal seizures and epilepsia partialis continua. The boy's overall condition slowly stabilized over several weeks, but he was left with severe rigidity and dystonic tetraparesis, profound mental retardation and drug-resistant epilepsy. MRI performed 4 months after onset of first symptoms revealed generalized cerebral volume loss. Treatment with biotin (7 mg/kg per day) and thiamine (100 mg per day) from age 9 years, after establishing the diagnosis of BTBGD, resulted in improved alertness and reduced seizure frequency.

His older brother (patient 2) presented at age 9½ years with a first episode of facial dyskinesia and dysarthria. Similar to his brother, MRI showed a high T2 signal in the basal ganglia with necrotic lesions in the caudate heads (Figure 1). A familial form of an acute necrotizing encephalopathy was discussed, but no further investigations were initiated, because his clinical symptoms resolved completely without specific treatment over 2 weeks. A control MRI 5 months later showed residual bilateral cystic lesions in the caudate head, while swelling and signal hyperintensities had regressed. At age 13½ years, he was re-admitted because of confusion, oral dyskinesia and dysarthria without a preceding illness. His symptoms progressed to generalized dystonia and rigidity with hypoventilation and dysphagia. He became comatose, showed dilated and fixed pupils, and developed epilepsia partialis continua. The onset of seizures was accompanied by occurrence of patchy cortical lesions in both hemispheres on MRI (Figure 1). The boy deceased 4 weeks after onset of symptoms because of respiratory insufficiency caused by status epilepticus in combination with aspiration pneumonia, before the diagnosis could be established. Neuroradiological investigations of both patients were re-evaluated after the older brother's death, and now, the diagnosis of BTBGD was strongly suspected because of the characteristic bilateral basal ganglia lesions and the evaluation of radiological changes during course.

Mutational analysis

SLC19A3 sequencing revealed the missense mutation c.280T>C (p.W94R) in both patients and in their mother (Figure 2A,B). Determination of relative copy numbers for each exon disclosed a heterozygous deletion of exon 5 in both patients. To determine the exact breakpoints and the extension of the deletion, we designed a forward primer starting at the end of exon 4 (Del-F: 5′AACT GGGACCTTCTGGGAGAGC) and a reverse primer starting at the beginning of exon 6 (Del-R: 5′CTCTTCCTCTGGGTGA GACACATC). Both long-range PCR primers amplified an 8898 kb product in controls, whereas samples of the patients and their two fathers produced double bands in agarose gel electrophoresis (Figure 2A,C). Sequence analysis of these PCR products revealed a deletion of 4175 kb, causing a frame shift with a premature termination codon (c.1173–3992_1314 + 41del4175, p.Q393*fs). Amplification and sequencing of *SLC19A3* cDNA verified the deletion (Figure 2D).

Brain pathology

The macroscopic findings from patient 2 revealed cystic and necrotic lesions and hemorrhage in the putamen, and lesions in the caudate nucleus and cortical layers with focal iron positive macrophages, indicative of old hemorrhage (Figure 3A). The histological examination confirmed a mixture of acute, subacute and chronic changes. Vacuolation of the brain parenchyma and presence of eosinophilic neurons also indicated acute cell damage. Abundant petechial perivascular hemorrhages were observed (Figure 3B). Analyses of semithin sections demonstrated breakdown of the blood–brain barrier with perivascular edema, hemorrhage and endothelial cell drop off with endothelial leakage

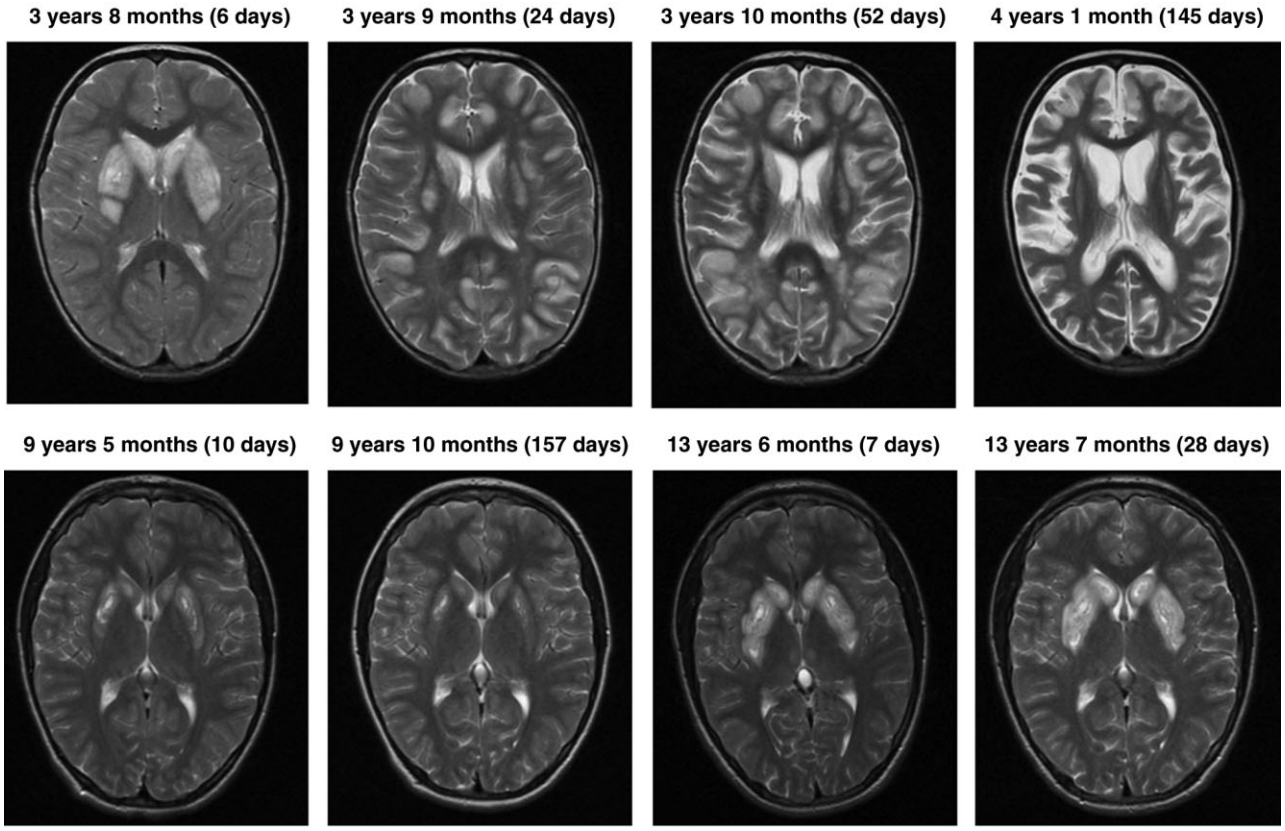

Figure 1. *Sequential T2-weighted axial magnetic resonance imaging (MRI) in patient 1 (upper panel) and patient 2 (lower panel).* Numbers in brackets correspond to days after clinical onset of an encephalopathic crisis. In patient 1, MRI at onset of the encephalopathic episode already demonstrates bilateral hyperintense swelling of the caudate head and putamen with central necrosis. Alterations are partially reversed after 24 days, while diffuse and progressive cortical lesions at the gray–white matter junction have appeared. Generalized enlargement of internal and external cerebrospinal fluid spaces without signal alterations is seen after 5 months. In patient 2, initial MRI during his first episode of encephalopathy reveals similar, but less severe basal ganglia injury compared with his brother. Changes have largely regressed 5 months later, but pronounced basal ganglia injury with increased signal intensity and swelling of the medial thalami re-occurred 4 years later (13 years 6 months).

(Figure 3C). Additionally, subacute and chronic changes with necrosis of the brain parenchyma and neovascularization as well as old cystic lesions were visible (Figure 3D,E). Moreover, semithin sections and electron microscopy of the basal ganglia showed acute necrotic neuronal changes (Figure 3F,G). Immunohistochemical staining for NeuN suggested severe neuronal loss in several cortical areas, mainly in layers II-IV, directly adjacent to areas with normal distribution of neurons (Figure 4A,B), whereas staining for GFAP showed reactive astrocytes in the parietal cortex (Figure 4C) and basal ganglia (Figure 4D). These findings were corroborated by Western blot of brain lysates demonstrating markedly decreased NeuN expression in the cortex and especially in the basal ganglia, while GFAP was normally expressed (Figure 6E). Histological and immunohistochemical stainings with lymphocytic antibodies (CD3, CD8, CD20 and CD45) revealed no signs of inflammation. Moreover, enzymatic (Gram, Ziehl-Neelsen, Grocoot) and immunohistochemical (antibodies against toxoplasma gondii and cytomegalovirus) analyses showed no evidence for an underlying pathogenic agent (data not shown).

Thiamine transporter activity and cellular localization of the BTBGD-associated SLC19A3 mutants

The p.W94R and the p.Q393*fs variant as well as the wt were cloned in the mammalian expression vector pcDNA5/FRT/V5-His expressing proteins with or without V5-His-tag. The concentration dependent uptake of thiamine (1 μM–75 μM) was measured after transient transfection of the respective plasmids (without tag) into GripTite 293 MSR cells (Figure 5A–C). The specific uptake of wt and p.W94R variant showed a saturation kinetic, which followed the Michaelis–Menten equation. The kinetic parameters revealed a similar capacity of both proteins, but a decreased affinity of p.W94R compared with wt*SLC19A3*. Strikingly, the p.Q393*fs mutation entirely abolished thiamine transport compared with control cells. Transfection of all V5-His tagged proteins in GripTite 293 MSR cells could be detected at similar levels and showed comparable transport activity to the respective untagged proteins (data not shown).

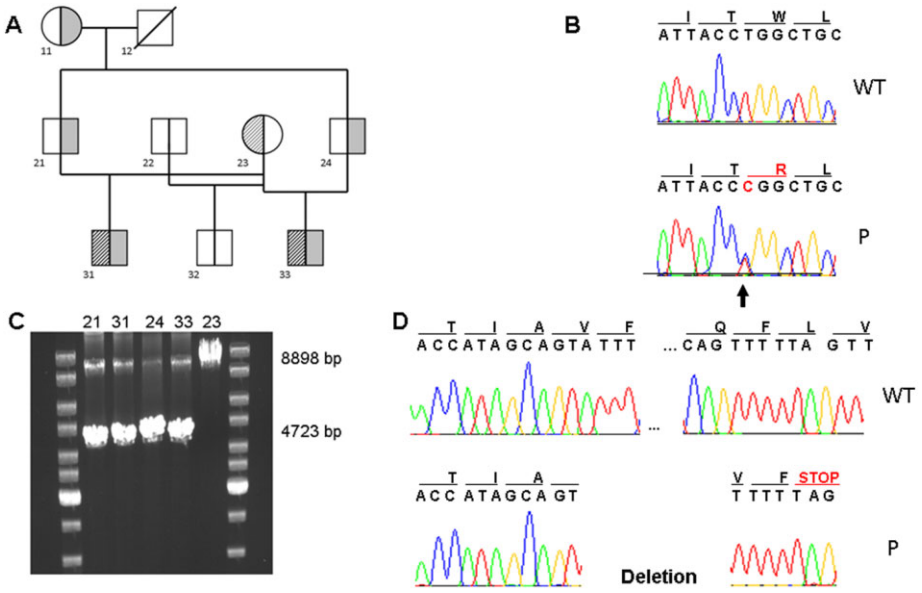

Figure 2. *Molecular genetic analyses.* **A.** Pedigree chart of the family. Gray-filled symbols correspond to subjects carrying the p.Q393*fs deletion and shaded ones represent individuals harbouring the p.W94R substitution. **B.** Electropherogram of patient 1 (P + 33) showing a heterozygous T to C exchange at position 280 (arrow) of the *SLC19A3* gene compared to the wild type (WT) sequence. **C.** Long-range polymerase chain reaction (PCR) of the parents and both patients, disclosing a 4175 kb large deletion of the *SLC19A3* gene in the two fathers (21 + 24) and in both patients (31 + 33), whereas the mother (23) exhibits a PCR fragment of normal length. **D.** Electropherogram of patient 2 (P) showing 5′start (position 1174) and 3′end (position 1314) of the deletion, which results in a stop codon at position 1319 (conform to amino acid 393) compared with the WT sequence.

Transfection of V5-His tagged wt and mt*SLC19A3* constructs into MDCK cells and analysis of their intracellular localization by immunofluorescence demonstrated that the wt and p.W94R mutant protein were localized both on the cell surface and in intracellular compartments. By contrast, no cell surface localization was observed for the p.Q393*fs mutant transporter (Figure 5D–F), explaining the complete blockade of thiamine uptake in GripTite 293 MSR cells. Accordingly, the p.W94R mutant and the wt showed transport activity in MDCK cells, whereas the p.Q393*fs mutant did not (data not shown).

Expression of mtSLC19A3 in different brain regions

Immunoblotting of protein lysates was performed from liver tissue and from different regions of the patient's and a control brain, including cortex, basal ganglia and the cerebellum. Analysis of the patient's brain revealed greatly reduced mtSLC19A3 protein levels compared with control (Figure 6A). This decrease was particularly striking in the basal ganglia and in the cortex, while the cerebellum was less affected. SLC19A3 antibodies were raised against a region neither affected by the p.W94R nor by the p.Q393*fs mutation (15). In addition, examination of *SLC19A3* expression at the mRNA level showed a strong downregulation of mt*SLC19A3* in the cortex, basal ganglia and cerebellum compared with control (Figure 6B), suggesting that the mutations also affect *SLC19A3* mRNA transcription or stability.

SLC19A3 Expression in wt and mt cells during hypoxia and acidosis

To test whether wt and mt*SLC19A3* respond differentially to stress stimuli, we incubated fibroblasts isolated from BTBGD patient 1 and from a control patient under conditions of hypoxia or acidosis, two microenvironmental factors linked to inflammatory processes and altered metabolism (8, 10). Hypoxia (1% O_2 for 18 to 96 h) induced a major upregulation of *SLC19A3* in control cells. By contrast, hypoxia had little effect on *SLC19A3* expression in the patient's cells (Figure 6C), indicating that the *SLC19A3* mutants cannot efficiently respond to reduced oxygen tension. Similarly, acidosis caused a prominent increase of wt*SLC19A3*, while levels in *SLC19A3* mutant cells remained unchanged (Figure 6D). Incubation of patient's fibroblasts with different biotin concentrations did not augment mt*SLC19A3* expression (data not shown).

DISCUSSION

Mutations in the *SLC19A3* gene are associated with an increasing spectrum of clinical phenotypes, ranging from Leigh-like syndrome in infants to BTBGD in children, and Wernicke's-like encephalopathy in young adults. Here, we assessed comprehensively the genetic, radiologic, post-mortem and functional data in a family with two brothers affected by BTBGD, in an attempt to elucidate how *SLC19A3* mutations lead to brain lesions and how extrinsic factors can trigger acute encephalopathic crises.

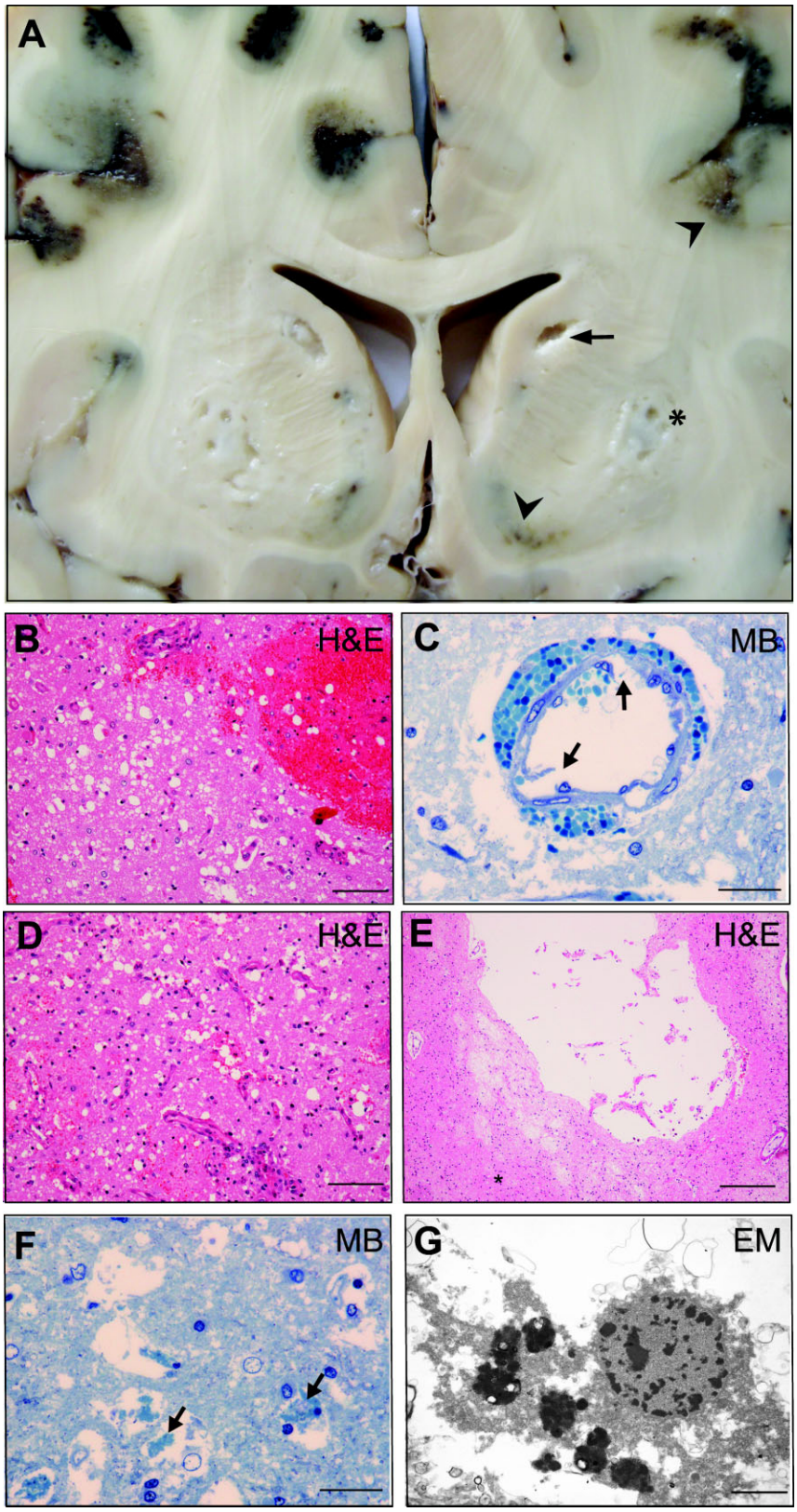

Figure 3. *Brain autopsy findings in patient 2.* **A.** Midfrontal section demonstrating acute hemorrhagic lesions in the caput nuclei caudati and cortical layer (arrowheads), subacute necrotic lesions in the putamen (asterix) and old cystic lesions in the caudate nucleus (arrow). **B.** Histology of the basal ganglia showing acute lesions with edema of the brain parenchyma with focal hemorrhage. **C.** Semithin section revealing vascular leakage, perivascular edema and hemorrhage caused by drop off of endothelial cells (arrows). **D,E.** Histology of the basal ganglia demonstrating subacute and chronic lesions with gliosis, neovascularization and old cystic areas. **F,G.** Semithin section and electron microscopy confirming acute neuronal damage (arrows). Bars= 200 μm in **B,D,E**; Bars= 50 μm in **C,F**.

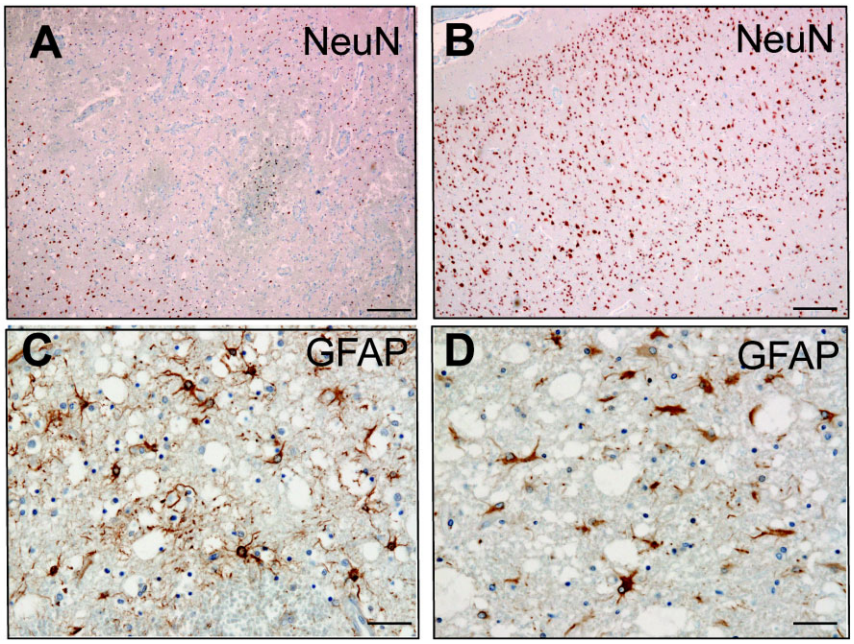

Figure 4. *Immunhistochemical findings in patient 2.* A–B. Severe loss of neurons (NeuN) in the parietal cortex **(A)** compared with adjacent areas of normal appearance **(B)**. C–D. Reactive astrocytes (GFAP) in the parietal cortex **(C)** and basal ganglia **(D)**. Bar =500 μm in A,B; Bar = 200 μm in C,D.

Mutational analysis revealed that our patients were compound heterozygous for one previously reported (p.Q393*fs) (7) and one novel (p.W94R) pathogenic *SLC19A3* variant, both leading to functional alteration of the protein. The p.W94R mutant has a 6.5-fold lower affinity to thiamine compared with wt, resulting in diminished transport activity at physiological thiamine concentrations. The p.Q393*fs mutant completely lacked thiamine transport activity and was not detectable at cell surface. These findings are in line with previous studies analyzing the functional consequences of *SLC19A3* mutations (p.S7Ter, p.G23V, p.K44E, p.E320Q and p.T422A), which all showed reduced or even absent thiamine transport activity (6, 11, 19, 22). In addition, protein and mRNA expression of *SLC19A3* were distinctly diminished in the patient's cortex and basal ganglia, indicating ubiquitously reduced *SLC19A3* function in the gray matter. The relative levels of *SLC19A3* between different tissues and brain regions showed some variability at the mRNA compared with the protein level (Figure 6A,B). These observations suggest differential regulation of *SLC19A3* at the mRNA and protein levels, e.g. as a result of different degradation kinetics or posttranscriptional/posttranslational control mechanisms for the mRNA transcript and its cognate protein.

In our patients, MRI in the initial stage demonstrated symmetric signal alterations and cystic changes of the caudate head and putamen, indicative of cytotoxic edema and neuronal necrosis (14, 21). These alterations partially reversed or progressed to extensive cortico-subcortical lesions in our untreated patients, while the late stage was characterized by generalized cortical atrophy without signal alterations. In addition to other neurological symptoms and radiological findings previously reported in BTBGD, epilepsia partialis continua constituted a major clinical problem in both our subjects. Neuropathological examinations which have not been reported in a patient with BTBGD confirmed the MRI findings. We observed a mixture of distinct acute, subacute and old lesions in the basal ganglia and cortical layer. Selective loss of neurons, endothelial leakage with hemorrhage, and disruption of the blood–brain barrier with pronounced neovascularization were the most prominent features. These findings are in principal congruence with the severe alterations recently reported by Kevelam and colleagues in two infants with *SLC19A3* mutations and a Leigh phenotype (9), suggesting that both phenotypes form a continuum within the spectrum of *SLC19A3*-associated disorders (9, 16). In the two patients with Leigh phenotype, staining with antibodies directed against *SLC19A3* revealed an increased expression in reactive astrocytes and in the wall of cerebral blood vessels, suggesting that intracellular thiamine levels affect THTR2 expression in these cell types (9). In addition, the authors detected no *SLC19A2*-positive astrocytes in the cerebral cortex of four deceased neurologically healthy infants, serving as controls (9). In our study, we did not specifically assess *SLC19A3* expression in blood vessels and astrocytes, but the results of our Western blot analysis and histopathological findings, demonstrating reduced expression of the neuronal marker NeuN and normal expression of the glial marker GFAP, are consistent with a largely specific involvement of neuronal cells by THTR2 deficiency. Although these results and the study of Kevelam strongly support a direct involvement of *SLC19A3* and intracellular thiamine deficiency in neuronal cell survival and function, it cannot be ruled out that neuronal loss occurring secondary to metabolic stress may also play a role.

Several metabolic diseases, e.g. glutaric aciduria type 1, methylmalonic acidemia, and 3-methylglutaconic aciduria, may manifest as acute or subacute necrotizing encephalopathies involving the basal ganglia (14). The differential diagnosis of BTBGD also includes mitochondrial disorders, in particular Leigh syndrome, which is characterized by bilateral necrotic lesions and vascular proliferations in the thalamus, basal ganglia, brain stem and spinal cord, while obvious involvement of the cortical gray

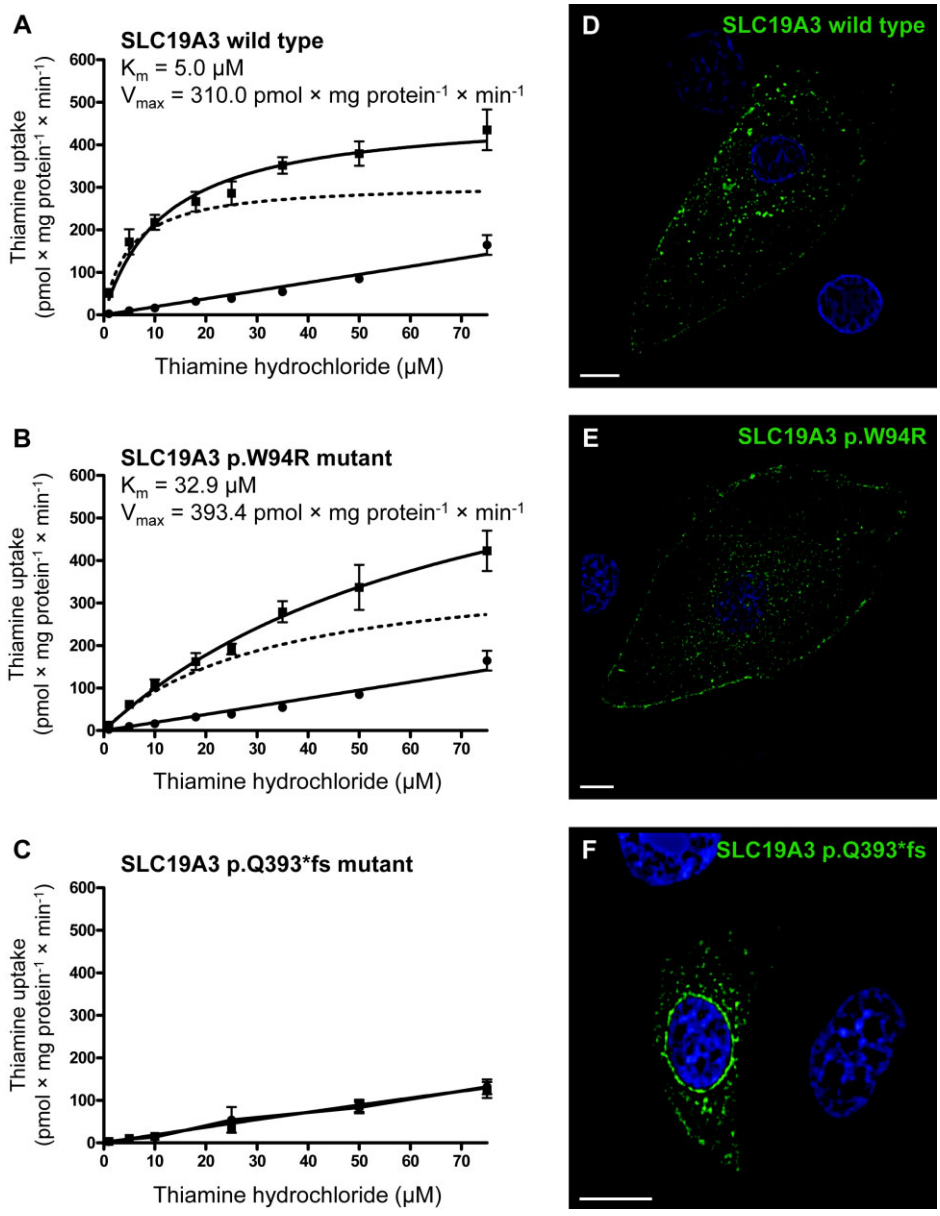

Figure 5. *Thiamine transporter 2 (THTR2) uptake studies.* **A–C.** Concentration dependent thiamine uptake (1 µM–75 µM) in MSR GripTite 293 cells transiently transfected with SLC19A3 wild type, SLC19A3 p.W94R mutant and SLC19A3 p.Q393*fs mutant (filled squares), and empty vector (control, filled circles) for 1 min. Transporter specific uptake was calculated by subtracting the uptake in the control cells from the uptake in the transporter transfected cells. Nonlinear regression analysis following the Michaelis–Menten equation was used to determine kinetic parameters (K_m, V_{max}) of transporter specific uptake (dashed line). **D–F.** Immunofluorescence studies of MDCK cells transiently transfected with V5-His tagged *SLC19A3* wild type, p.W94R mutant or p.Q393*fs mutant. The V5-epitope was detected using mouse anti-V5 primary antibody and goat anti-mouse IgG AF488 secondary antibody (green fluorescence). Cell nuclei were visualized with DAPI (blue fluorescence). Bars = 10 µm in **D,E,F**.

matter or hemorrhage is usually not observed (5). Therefore, hemorrhagic lesions of the basal ganglia and early cortical involvement as seen in our patient seem to represent typical features of SLC19A3-related disorders, which may help to distinguish them from other necrotizing encephalopathies. Biotinidase deficiency may manifest as a subacute encephalopathy often with seizures as a prominent finding, which is also potentially reversible if higher doses of biotin are administered timely. But unlike BTBGD, cerebral volume loss, delayed myelination and subacute demyelination also involving the spinal cord and brain stem are characteristic signs, whereas basal ganglia involvement is uncommon (3).

Conversely, the macroscopic and microscopic findings in our patient with endothelial leakage and hemorrhage appear similar

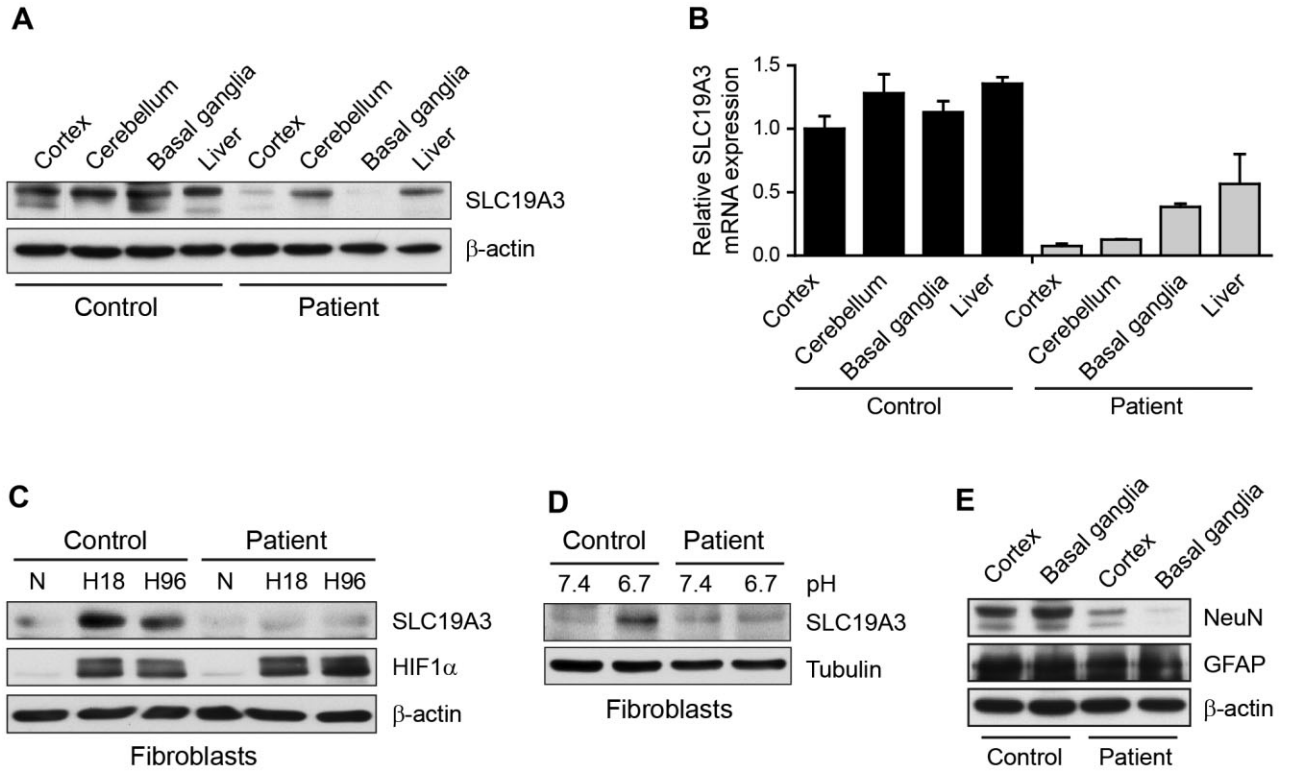

Figure 6. *SLC19A3 expression and regulation by hypoxia and acidosis.* **A–B.** Western blot and real-time polymerase chain reaction (PCR) analysis of *SLC19A3* expression in different parts of the brain and in the liver of patient 2 and in a control patient of same age, demonstrating substantially reduced *SLC19A3* expression in all cerebral regions in the patient. **C–D.** Western blot analysis of *SLC19A3* expression in the patient's and in healthy control's fibroblasts under hypoxic (1% O_2 for 18 or 96 h) and acidotic conditions (pH 6.7 for 24 h). **E.** Expression of the neuronal marker NeuN and the glial marker GFAP in cortex and basal ganglia of patient 2 and in the control patient, indicating selective neuronal loss in the patient. β-actin and tubulin served as loading controls.

to those observed in Wernicke's encephalopathy (WE), a neuropsychiatric disorder caused by nutritional thiamine deficiency (4, 8, 13, 16, 24). While in adults with WE, such lesions are typically restricted to the mammillary bodies, tectal plate, periaqueductal area and medial portions of the thalami; additional involvement of the putamen, caudate nucleus and cortex, as observed in BTBGD, is not infrequent in pediatric cases (24).

Repeated descriptions have emphasized that a preceding illness or a catabolic state provoked a first episode of encephalopathy in hitherto normal subjects with BTBGD (2, 14, 18). One possible explanation for this observation is that stress stimuli induced during such periods modulate the activity of wt*SLC19A3*, whereas mutant transporters are less responsive to such factors. Interestingly, breast cancer cells exposed to chronic hypoxia were found to show an approximately 40-fold increase of *SLC19A3* expression with no change in *SLC19A2* expression (20). Our results demonstrate that hypoxia-induced upregulation of *SLC19A3* expression also occurs in wild type human non-neoplastic cells. Notably, *SLC19A3* levels were similarly elevated by acidosis, which is associated with hypoxia and other stress stimuli such as inflammation and metabolic shift; stimuli that can also be induced by thiamine deficiency (4, 15). Conversely, the markedly diminished induction of *SLC19A3* expression in the mutant cells is compatible with the hypothesis of a substantially limited capacity of *SLC19A3*-deficient neuronal cells to adapt to cellular stress (Figure 6). To our knowledge, similar experiments in other disorders associated with clinical deterioration during an acute illness have not been performed.

In nutritional thiamine deficiency, reduction of α-ketoglutarate dehydrogenase activity, a thiamine diphosphate dependent enzyme, is associated with potentially reversible mitochondrial dysfunction and lactic acidosis (4, 15). As in our cases, most studies reporting older children affected by THTR2 deficiency found no biochemical abnormalities indicating impaired mitochondrial function. However, reduced respiratory chain enzyme activities in muscle, lactic acidosis and increased α-ketoglutarate excretion have been recently reported in infants with *SLC19A3* mutations and a Leigh-like phenotype (6, 9, 16), thus linking impaired thiamine transporter capacity to mitochondrial dysfunction.

The results of our thiamine uptake studies lend further support to the crucial rule of thiamine in the treatment of patients with *SLC19A3* deficiency, but suggest that response to therapy may also depend on specific *SLC19A3* mutations. While it seems unlikely that administration of thiamine is of substantial benefit in case of

completely abolished transporter function, this treatment should be meaningful if the transport capacity is reduced at physiological concentrations. While several studies made plausible why thiamine treatment is important in THTR2 deficiency, it is unclear how administration of high-dose biotin can improve neurological symptoms in some patients (2). In our study, incubation of patient and wt fibroblasts with different biotin concentrations when exposed to hypoxia and stress, did not augment *SLC19A3* gene expression in mutant or in wt fibroblasts. These negative findings are in line with the study of Alfadhel and colleagues who retrospectively analyzed 18 patients with THTR2 deficiency. They found that one-third showed recurrence of acute crises when treated with biotin alone, whereas no further encephalopathic episodes occurred after thiamine was added (1).

In conclusion, this study provided further evidence that BTBGD is the result of a reduced thiamine transport activity in neuronal cells, and suggests that impaired stress-mediated induction of mutant *SLC19A3* plays a key role in triggering episodes of encephalopathy in patients with THTR2 deficiency. Our neuropathological findings confirmed the results of the thiamine uptake studies and the neuradiological examinations. They also support the hypothesis that the different phenotypes associated with *SLC19A3* deficiency are distinct parts of a spectrum, depending largely on the regional variations in energy metabolism at different ages (16).

ACKNOWLEDGMENTS

We thank S. Gräf-Höchst, G. Schmidt, N. Rötering and C. Dambmann for technical assistance.

REFERENCES

1. Alfadhel M, Almuntashri M, Jadah RH, Bashiri FA, Al Rifai MT, Al Shalaan H *et al* (2013) Biotin-responsive basal ganglia disease should be renamed biotin-thiamine-responsive basal ganglia disease: a retrospective review of the clinical, radiological and molecular findings of 18 new cases. *Orphanet J Rare Dis* **8**:83. doi: 10.1186/1750-1172-8–83.
2. Debs R, Depienne C, Rastetter A, Bellanger A, Degos B, Galanaud D *et al* (2010) Biotin-responsive basal ganglia disease in ethnic Europeans with novel SLC19A3 mutations. *Arch Neurol* **67**:126–130.
3. Desai S, Ganesan K, Hegde A (2008) Biotinidase deficiency: a reversible metabolic encephalopathy. Neuroimaging and MR spectroscopic findings in a series of four patients. *Pediatr Radiol* **38**:848–856.
4. Desjardins P, Butterworth RF (2005) Role of mitochondrial dysfunction and oxidative stress in the pathogenesis of selective neuronal loss in Wernicke's encephalopathy. *Mol Neurobiol* **31**:17–25.
5. Ellison D, Love JS (2013) Leigh's disease (subacute necrotising encephalomyopathy). Chapter 6. In: *Neuropathology. A reference text of CNS pathology*, 3rd edn. D Ellison, S Love, LM Chimelli, B Harding, JS Lowe, HV Vinters *et al* (eds), pp. 150–152. Mosby Elsevier Limited: St. Louis, MO.
6. Gerards M, Kamps R, van Oevelen J, Boesten I, Jongen E, de Koning B *et al* (2013) Exome sequencing reveals a novel Moroccan founder mutation in SLC19A3 as a new cause of early-childhood fatal Leigh syndrome. *Brain* **136**:882–890.
7. Geyer J, Döring B, Meerkamp K, Ugele B, Bakhiya N, Fernandes CF *et al* (2007) Cloning and functional characterization of human sodium-dependent organic anion transporter (SLC10A6). *J Biol Chem* **282**:19728–19741.
8. Hazell AS, Butterworth RF (2009) Update of cell damage mechanisms in thiamine deficiency: focus on oxidative stress, excitotoxicity and inflammation. *Alcohol Alcohol* **44**:141–147.
9. Kevelam SH, Bugiani M, Salomons GS, Feigenbaum A, Blaser S, Prasad C *et al* (2013) Exome sequencing reveals mutated SLC19A3 in patients with an early-infantile, lethal encephalopathy. *Brain* **136**:1534–1543.
10. Kominsky DJ, Campbell EL, Colgan SP (2010) Metabolic shifts in immunity and inflammation. *J Immunol* **184**:4062–4068.
11. Kono S, Miyajima H, Yoshida K, Togawa A, Shirakawa K, Suzuki H (2009) Mutations in a thiamine-transporter gene and Wernicke's-like encephalopathy. *N Engl J Med* **360**:1792–1794.
12. Majmundar AJ, Wong WJ, Simon MC (2010) Hypoxia-inducible factors and the response to hypoxic stress. *Mol Cell* **40**:294–309.
13. Okeda R, Taki K, Ikari R, Funata N (1995) Vascular changes in acute Wernicke's encephalopathy. *Acta Neuropathol* **89**:420–424.
14. Ozand PT, Gascon GG, Al Essa M, Joshi S, Al Jishi E, Bakheet S *et al* (1998) Biotin-responsive basal ganglia disease: a novel entity. *Brain* **121**:1267–1279.
15. Pannunzio P, Hazell AS, Pannunzio M, Rao KV, Butterworth RF (2000) Thiamine deficiency results in metabolic acidosis and energy failure in cerebellar granule cells: an *in vitro* model for the study of cell death mechanisms in Wernicke's encephalopathy. *J Neurosci Res* **62**:286–292.
16. Pérez-Dueñas B, Serrano M, Rebollo M, Muchart J, Gargallo E, Dupuits C *et al* (2013) Reversible lactic acidosis in a newborn with thiamine transporter-2 deficiency. *Pediatrics* **131**: e1670–e1675.
17. Said HM, Balamurugan K, Subramanian VS, Marchant JS (2004) Expression and functional contribution of THTR-2 in thiamine absorption in human intestine. *Am J Physiol Gastrointest Liver Physiol* **286**:G491–G498.
18. Serrano M, Rebollo M, Depienne C, Rastetter A, Fernández-Álvarez E, Muchart J *et al* (2012) Reversible generalized dystonia and encephalopathy from thiamine transporter 2 deficiency. *Mov Disord* **27**:1295–1298.
19. Subramanian VS, Marchant JS, Said HM (2006) Biotin-responsive basal ganglia disease-linked mutations inhibit thiamine transport via THTR2: biotin is not a substrate for THTR2. *Am J Physiol Cell Physiol* **291**:C851–C859.
20. Sweet R, Paul A, Zastre J (2010) Hypoxia induced upregulation and function of the thiamine transporter, SLC19A3 in a breast cancer cell line. *Cancer Biol Ther* **10**:1101–1111.
21. Tabarki B, Al-Shafi S, Al-Shahwan S, Azmar Z, Al-Hashem A, Al-Adwani N *et al* (2013) Biotin-responsive basal ganglia disease revisited: clinical, radiologic, and genetic findings. *Neurology* **80**:261–267.
22. Yamada K, Miura K, Hara K, Suzuki M, Nakanishi K, Kumagai T *et al* (2010) A wide spectrum of clinical and brain MRI findings in patients with SLC19A3 mutations. *BMC Med Genet* **11**:171.
23. Zeng WQ, Al-Yamani E, Acierno JS Jr, Slaugenhaupt S, Gillis T, MacDonald ME *et al* (2005) Biotin-responsive basal ganglia disease maps to 2q36.3 and is due to mutations in SLC19A3. *Am J Hum Genet* **77**:16–26.
24. Zuccoli G, Siddiqui N, Bailey A, Bartoletti SC (2010) Neuroimaging findings in pediatric Wernicke encephalopathy: a review. *Neuroradiology* **52**:523–529.